

# Shark Body Shape Evolution: Adaptations in Locomotion Across the Benthic-Pelagic Habitat Axis

xx

*Keywords:* Selachians, morphospace, Ornstein-Uhlenbeck, ecomorphology, evolutionary rates.

## Abstract

Ecological transitions are fundamental drivers of macroevolutionary patterns in form. We investigated how transitions in habitat across the benthic-to-pelagic axis have influenced the evolution of body shape in sharks (Selachii). Drawing on morphological data important to locomotor behavior and performance from 288 extant species and a time-calibrated molecular phylogeny, we evaluated if habitat drives differences across multivariate and univariate trait space, evolutionary rates, and phenotypic optima. Our analyses reveal that while multivariate body shape overlaps substantially among habitats, certain traits including caudal fin morphology and the positions of paired fins exhibit significant variation aligned with habitat use. We recovered a benthic-to-pelagic gradient in trait optima and evolutionary rates. Pelagic sharks have posteriorly displaced fins, broader caudal surfaces, and lower evolutionary rates for these key locomotor traits. These patterns suggest that the ecological demands of pelagic life constrain morphological diversification, while benthic habitats promote it. Furthermore, reconstructions of ancestral habitat states indicate multiple independent transitions into pelagic environments, particularly within carcharhiniforms, challenging previous hypotheses about the timing and drivers of these ecological shifts. Altogether, our results underscore habitat's central role in shaping shark body plans and highlight a macroevolutionary trade-off between ecological specialization and phenotypic diversity.

## Introduction

The evolutionary interplay between organismal shape and habitat is well established, particularly in aquatic vertebrates, where body forms evolve to enhance locomotion, foraging, and reproduction in response to habitat-specific environmental constraints (Burress et al., 2017; Friedman et al., 2020; Hulsey et al., 2013; Martinez et al., 2021; Miller et al., 2025; Ribeiro et al., 2018). Several studies have emphasized the historical role of habitat in shaping shark body morphology, focusing on key adaptations to the hydrodynamic and ecological demands of benthic and pelagic environments (Fish & Shannahan, 2000; Gayford et al., 2023; Gleiss et al., 2017; López-Romero et al., 2023; Sternes et al., 2024; Sternes & Shimada, 2020; Thomson & Simanek, 1977). Benthic species typically exhibit dorsoventrally flattened bodies and broad pectoral fins, enhancing station-holding, maneuverability, and camouflage near the substrate (Sternes & Shimada, 2020; Thomson & Simanek, 1977). In contrast, pelagic sharks are characterized by deep, fusiform bodies, high-aspect-ratio pectoral fins, and heterocercal tails that facilitate sustained, efficient swimming and prey capture in the open ocean (Sternes et al., 2024; Sternes & Shimada, 2020; Thomson & Simanek, 1977).

Despite a considerable body of work that outlines drivers of shark body shape evolution, no single study has explicitly addressed macroevolutionary patterns of body shape variation in relation to habitat use across the shark phylogeny. In their classic study, Thomson & Simanek (1977) outlined four major body shape configurations in sharks, each largely associated with specific habitats: pelagic, fast-swimming sharks (e.g., *Isurus*, *Lamna*) with high-aspect ratio caudal fins and narrow peduncles; generalist sharks (e.g., *Carcharhinus*) with moderate heterocercal angles and long, robust pectoral fins; benthic sharks (e.g., *Ginglymostoma*) with swept dorsal caudal lobes and reduced ventral caudal lobes; and squalomorphs (e.g., *Squalus*) with high-set pectorals and somewhat elongated ventral caudal lobes. Sternes & Shimada (2020) conducted a comprehensive geometric morphometric analysis of a majority of shark species (~470 species) and outlined major patterns in the relationships among body shape, locomotor mode, and habi-

tat. In contrast to Thomson & Simanek (1977), they identified two primary body types: Group A sharks, which are typically benthic and exhibit anguilliform (eel-like) swimming; and Group B sharks, which are often pelagic and swim using carangiform or thunniform modes. Although precaudal shape correlated strongly with habitat and swimming mode, caudal fin morphology showed no consistent pattern. While both studies represent important contributions to our understanding of shark ecomorphology, Thomson & Simanek (1977) included fewer than 60 species in their analysis and Sternes & Shimada (2020) did not explicitly test assess the effects of habitat on body shape variation within a comparative macroevolutionary framework.

More recently, Sternes et al. (2024) investigated evolutionary shifts from benthic to pelagic habitats with a focus on pectoral-fin morphology. They found that pelagic sharks evolved independently from benthic or benthopelagic ancestors and that transitions to pelagic habitats were typically associated with the evolution of long, narrow pectoral fins. These changes were interpreted as adaptations to the locomotor constraints of open water, where sustained swimming and lift generation are required in the absence of a substrate. This study did not, however, consider how other key control surfaces (e.g., dorsal, pelvic, and caudal fins) evolve in response to habitat shifts.

Although previous studies have described general patterns of body shape evolution associated with water-column habitat preferences, no single analysis has systematically tested how habitat influences shark body morphospace across the shark phylogeny. Here, we analyze habitat-mediated diversification of body shape across 288 species of extant sharks, representing more than half of the taxonomically valid species (Ebert et al., 2021). We integrate morphometric, habitat, and phylogenetic data in a comparative methods framework to investigate how habitat gradients influence differences in morphospace, rates of phentotypic evolution, and trait-specific phenotypic optima. We hypothesize that the pelagic environment, characterized by physical and ecological homogeneity, imposes strong constraints on body shape and rates of morphological evolution, resulting in the evolution of key locomotor designs that promote efficient cruising and foraging in this homogeneous environment. In contrast, we expect benthic and benthopelagic

sharks to exhibit greater rates of morphological evolution associated with locomotor versatility and bottom-associated behaviors.

## Methods

### *Software and Code*

All analyses were conducted using custom scripts written in R (R Core Team, 2022) and, unless otherwise noted, all software packages were written for this environment. Scripts and data are available at [http://datadryad.org/share/sKBbmG5G6K\\_7vPrCPMU0ickRCAomCgj44WLUuuHYhI](http://datadryad.org/share/sKBbmG5G6K_7vPrCPMU0ickRCAomCgj44WLUuuHYhI).

### *Data Collection*

We selected species included in the molecular phylogeny of Stein et al. (2018) and illustrated by (Ebert et al., 2021, hereafter Ebert). Following Sternes & Shimada (2020) and Sternes et al. (2024), we collected Ebert's illustrations for all species in the Stein et al. (2018) phylogeny and then digitized 12 homologous landmarks with FIJI (Schindelin et al., 2012). From these, we calculated 13 linear variables (Figure S1): precaudal length (PCL), body depth, dorsal- and pectoral-fin base lengths, pre-dorsal and pre-pectoral-fin lengths, dorsal-fin length, dorsal and ventral caudal-lobe lengths, and caudal angle (the sum of heterocercal and hypochordal angles). Because some shark lineages lack a second dorsal (hexanchiforms and pristiophoriforms) or anal fin (squaliforms), we omitted these fins from analysis.

Most species in Ebert are drawn in lateral view, except squatiniforms, which are depicted in dorsal view with caudal fins rotated into lateral view. This allowed measurement of all traits except body depth. For this, we used head depth from the anterior-view drawing as a proxy, assuming this reflects overall body depth in this dorsoventrally compressed group.

This process resulted in a dataset of 288 of the 292 species in Stein et al. (2018). Three squatiniforms lacked anterior head views, preventing body depth measurement, and *Glyptis*

*fowlerae* was not included in Ebert. These 288 species represent over half of the 530 extant, valid shark species, all nine extant selachian orders, 37 of 39 families, and 93 of 107 genera (Ebert).

Habitat assignments followed descriptions in Ebert and Compagno (1984, hereafter Compagno”), using keywords like “bottom dwelling” or “on seabed” for benthic, and “midwater,” “pelagic,” “epipelagic,” “mesopelagic,” or “bathypelagic” for pelagic. Benthopelagic species were identified by terms such as “near bottom,” “off bottom,” or “demersal.” Classifications were compared with Sternes et al. (2024) and discrepancies were reviewed in detail.

We downloaded 500 time-calibrated molecular phylogenies for chondrichthyans from [vertlife.org](http://vertlife.org) (Stein et al., 2018), pruned them to the 288 study species, and computed a strict consensus tree with mean edge lengths using `consensus.edges` in `phytools` (Revell, 2024). Because tree topologies were identical, this yielded a fully resolved, dichotomous tree. This approach is more conservative than that of Sternes & Shimada (2020), who used a maximum clade credibility (MCC) tree generated from a taxonomically resolved set of 10,000 trees. This phylogenetic hypotheses was constructed by adding species lacking molecular data using a polytomy-resolver algorithm (see Stein et al., 2018). By using a tree that included only taxa with molecular data, we reduced phylogenetic uncertainty in our study at the cost of excluding many species.

After  $\log_{10}$ -transformation, the twelve body-shape variable were regressed against  $\log_{10}$  PCL with phylogenetic generalized least squares (PGLS) models in the `nlme` package (Pinheiro & Bates, 2000) under both Brownian motion (BM) and Ornstein Uhlenbeck (OU) correlations structures. Best-fitting models were selected using AICc and the residuals were retained for comparative analyses. To assess allometry, we calculated the scaling coefficient  $b$  as the slope of each  $\log_{10}$ - $\log_{10}$  regression.

### *Habitat History Reconstruction*

We fit models of discrete habitat-state evolution using the `fitDiscrete` function in the `geiger` package (Garland Jr et al., 1993; Pennell et al., 2014). We compared three models: equal rates (ER), symmetrical (SYM), and all-rates-different (ARD). The best-fitting model based on AICc

weights was then used to generate 500 stochastic character maps ("simmmaps" hereafter) with the `phytools` function `simmap`. We summarized character maps to estimate the mean number and direction of transitions among habitat states and visualized these transitions using chord diagrams. Node states were inferred by calculating the maximum posterior probability across the 500 mappings. These most probable node states were then used to estimate the most probable number of transitions and their timings by identifying branches that lead to nodes of different states than the parent node. To assess the combined influence of our phylogenetic hypothesis and habitat classification, we repeated the analysis using the MCC tree of Stein et al. (2018) and our habitat designations, allowing comparison with the framework used by Sternes et al. (2024).

### *Morphospace and Rates of Phenotypic Evolution*

We examined morphological variation across habitats by performing a principal component analysis (PCA) on the correlation matrix of the 12 morphological variables and visualizing morphospace occupancy by habitat group. We tested for multivariate differences in mean shape among habitats via simulation-based phylogenetic MANOVA under a BM model using the `aov.phylo` function in `geiger`. We also conducted simulation-based phylogenetic ANOVAs for each morphological trait with post hoc-pairwise comparisons using the `phylANOVA` function in `phytools`. Post-hoc P values were adjusted using the false-discovery-rate method (`p.adjust = "fdr"`), a less conservative alternative to a Bonferroni correction (Pike, 2011). We assessed differences in net rates of multivariate and univariate trait evolution for all 12 traits according to habitat under a Brownian motion model of evolution using the `compare.evol.rates` function in the `geomorph` package (Baken et al., 2021). This approach also employs a simulation procedure to determine whether relative ratios of net diversification are significant. For all three of these analyses, we performed 10,000 simulations.

## *Macroevolutionary Model Fitting*

We employed a model-fitting framework to evaluate if water-column habitat is implicated in the evolution of different adaptive peaks (i.e., optima) and rates of phenotypic evolution across the shark phylogeny. To assess this, we used the `OUwie` package (Beaulieu & O'Meara, 2024) to construct five evolutionary models for each univariate trait. We first considered two BM models: BM1 assumes a single evolutionary rate ( $\sigma^2$ ) across all lineages, while BMS allows different rate parameters for each habitat regime. We also considered three OU variants that implement a single value for  $\alpha$ , the strength of selection: OU1, which assumes constant values of  $\sigma^2$  and  $\theta$ , the trait optimum, across all habitat regimes; OUM, which allows  $\theta$  to vary among habitat states; and OUMV which allows  $\theta$  and  $\sigma^2$  to vary among habitat states. Although more complex OU models that allow  $\alpha$  to vary can be implemented, our question focuses specifically on rates of phenotypic evolution and adaptive optima in the evolution in shark body shape. Furthermore, when  $\alpha$  is allowed to vary, interpretation of  $\sigma^2$  cannot be isolated from the strength of selection,  $\alpha$  (Cooper et al., 2016; Ho & Ané, 2014).

Due to the rather larger number of univariate traits and the computational complexity of these models, we limited model-fitting to those traits for which we found at least one significant pairwise difference between habitats in our phylogenetic ANOVAs of mean trait values or analyses of phenotypic evolutionary rates. We iteratively fit each model to each univariate trait using all 500 trees from our `simmap` analysis. We then used the median AICc score to rank these models and determine the best-fitting model for each univariate trait. For any trait, if any models were within 2 AICc units of the best-fitting model, we considered these models equivalent and also best-fitting. Parameter estimates from the best-fitting models were retained for interpretation.

We also assessed whether our models converged on reliable parameter estimates by evaluating if they produced positive eigenvalues (Beaulieu & O'Meara, 2024). In addition, because of the limited number of independent origins of pelagic ecology across the shark phylogeny (Sternes

et al., 2024) and the tendency of OUwie to favor overly complex models (Boettiger et al., 2012; Ho & Ané, 2014), we took a simulation approach to evaluate whether we had significant power to accurately distinguish the simpler BM models from the more complex OU models. Using the function `OUwie.sim`, we simulated 100 datasets for each univariate trait under each of the five models using the parameter estimates of the best-fitting model retained from our empirical analyses. We then ran the OUwie analysis on our simulated datasets for each trait using the same random sample of 100 simmap trees to determine whether the best-fit model for each trait could be recovered and that the model produced similar parameter estimates.

After ensuring that our models returned reliable parameter estimates and that we had the appropriate statistical power, we assessed whether the distribution of  $\theta$  and  $\sigma^2$  estimates were significantly different between habitat regimes. With any morphological variable for which OUM or OUMV fit best, we subjected their estimates of  $\theta$  to a one-way analysis of variance with habitat regime as a predictive variable and a subsequent Tukey's honest significance test (THSD). We repeated this procedure on  $\sigma^2$  in cases where BMS or OUMV fit best.

## Results

### *Body Shape Allometry*

According to our PGLS model fitting, we found that a BM correlation structure fit best for 11 of the morphological variables and an OU model fit best for caudal angle (all AIC weights = 1; Figure S2; Table S1). For all of the 12  $\log_{10}$ -transformed variables, there was a significant relationship with  $\log_{10}$  PCL. Half of the variables are isometric ( $b \sim 1.0$ ), including body depth, pectoral base length, peduncle depth, and pre-dorsal, pre-pectoral, and pre-pelvic lengths. A few variables scale positively ( $b > 1$ ), including dorsal and ventral caudal lobe lengths ( $b=1.06$  and 1.14, respectively), dorsal fin length ( $b=1.09$ ), pelvic base length ( $b=1.06$ ), and dorsal base length ( $b=1.09$ ). Caudal angle was the one variable that scales negatively ( $b=0.15$ ).

## *Habitat Classification and Transitions*

Of our 288 study species, we classified 116 as benthic, 131 as benthopelagic, and 41 as pelagic. This contrasts the habitat designations of the same species by Sternes et al. (2024) who classified 171 as benthic, 61 as benthopelagic, and 52 as pelagic. Four species included in this study were not included in Sternes et al. (2024).

A SYM model of discrete character evolution fit our habitat data best. Using this model to produce 500 stochastic character maps, we found a mean of 70.1 transitions between habitat states (Figure 1). Of these transitions, 28.6 are from benthic to benthopelagic, 20.0 are benthopelagic to benthic, 16.3 are benthopelagic to pelagic, and 5.16 are from pelagic to benthopelagic (Figure 1B). We recovered no transitions from benthic to pelagic nor from pelagic to benthic in our simmap analysis. The root node was recovered as benthic in 90.8% and benthopelagic in 9.2% of the simmap reconstructions, indicating a high probability that the former is the ancestral habitat of selachians (Figure 1A). Based on the most probable node states, we estimate that selechians have undertaken 12 independent transitions to the benthic realm, 24 independent transitions to the benthopelagic, and 15 to the pelagic.

After repeating our simmap analysis and ancestral state reconstructions using our habitat designations and the MCC tree used by Sternes et al. (2024), we infer that sharks undertook a mean of 72.2 transitions between habitat states (Figure S3). Of these transitions, 28.1 are from benthic to benthopelagic, 20.8 are benthopelagic to benthic, 17.3 are benthopelagic to pelagic, and 6.11 are from pelagic to benthopelagic (Figure S3B). We recovered essentially no transitions from benthic to pelagic and from pelagic to benthic in our simmap analysis (0.04 and 0.006, respectively). The root node was recovered as benthic in 91.2% and benthopelagic in 8.8% of these repeated simmap reconstructions, again indicating a high probability that benthic is the ancestral habitat of selachians (Figure S3A). Based on the most probable node states using the MCC tree, we estimate that selechians have undertaken 13 independent transitions to the benthic realm, 23 independent transitions to the benthopelagic, and 65 to the pelagic.

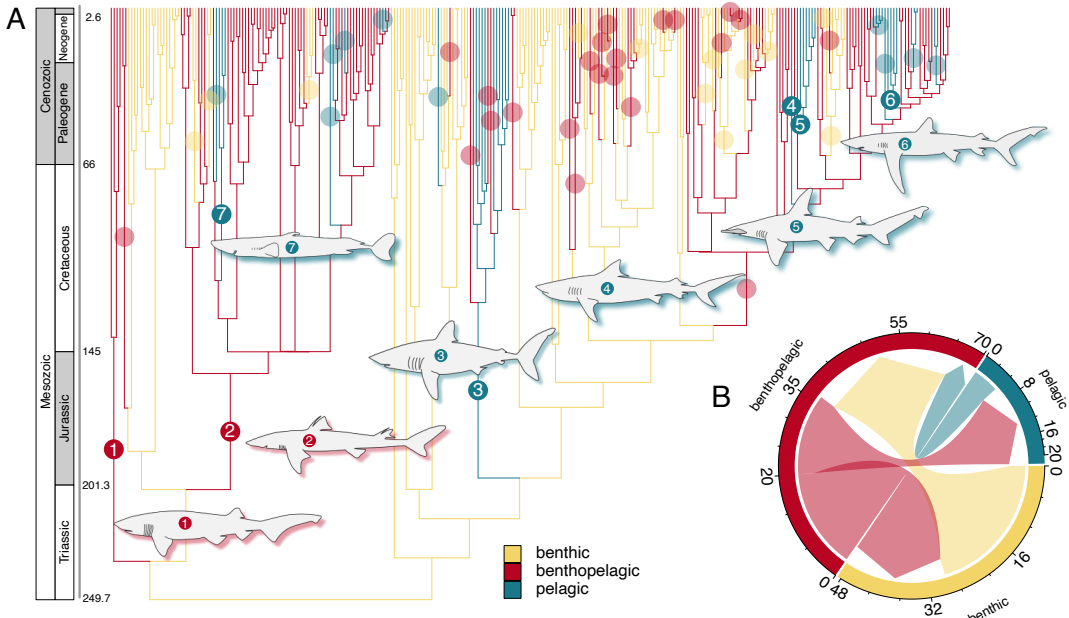


Figure 1: (A) Strict-consensus, fossil-calibrated time tree with mean edge lengths from (Stein et al., 2018). Edge colors represent habitat states and transparent circles represent state transitions across the phylogeny based on ancestral state reconstructions from 500 simmap procedures. Opaque, numbered circles represent major habitat transitions: 1, a benthopelagic transition in the branch leading to the Hexanchiformes; 2, a benthopelagic transition in the branch leading to the Squaliformes; 3, pelagic transition in the branch leading to the Laminiformes minus *Mitsukurina*; 4, pelagic transition in the branch leading to the genus *Sphyraena*; 5, a pelagic transition in the branch leading *Galeocerdo cuvier*, 6, a pelagic transition in the branch leading to a clade of *Prionace glauca* and several species of the genus *Carcharhinus*; and 7, a pelagic transition in the branch leading to a clade of deep-sea squaliforms of the genera *Euprotomicrus* and *Squaliolus*. Body-outline drawings represent species included in lineages that have undergone each of the major habitat shifts. (B) Chord diagram representing the the mean number of transition into and out of each habitat state from the 500 simmap trees.

### *Morphospace and Rates of Phenotypic Evolution*

The first three principal component (PC) axes accounted for 64.1% of the variation in body shape across the sampled sharks species (Figure 2). PC1 (31.2% of variance) was primarily influenced by differences in body depth, dorsal fin position and shape (length and base length), and pelvic

base length. PC2 (18.4% of variance) was dominated by variation in peduncle depth, dorsal and ventral caudal lobe length, pectoral base length. PC3 (14.5% of variance) was primarily associated with pre-pectoral and pre-pelvic lengths.

Overall, the morphospace defined by the first three PCs indicates broad overlap among benthic, benthopelagic, and pelagic species; however, some distinct patterns emerge (Figure 2). In the morphospace defined by PC1 and PC2 (49.6% of variance), many pelagic species (mostly carcharhiniforms) exhibit deeper bodies and longer dorsal fins (Figure 2A). In the PC1-PC3 morphospace (45.7% of variance), benthopelagic and especially pelagic species tend to have greater longer pre-pelvic lengths (Figure 2B). In the PC2-PC3 morphospace (32.9% of variance), benthic species tend to have longer pre-pectoral lengths (Figure 2C).

Our simulation-based phylogenetic MANOVA revealed significant multivariate morphological differences among habitat groups ( $F=10.4$ ,  $P=0.0058$ ). Simulation-based phylogenetic ANOVAs identified significant pairwise differences in 4 of the 12 morphological variables analyzed (see Table S2 for details and full pairwise comparisons). Mean body depth was significant between benthic and pelagic species, as well as between benthopelagic and pelagic species (both  $P=0.024$ ). Mean caudal ventral lobe length and pre-pectoral length were significantly different between benthic and pelagic species ( $P=0.033$  and  $0.037$ , respectively). The mean difference in pre-pelvic length was significant between benthic and benthopelagic species and between benthic and pelagic species ( $P=0.002$  and  $P<0.001$ , respectively).

Rates of multivariate phenotypic evolution varied significantly between water-column habitats ( $Z=3.49$ ,  $P<0.001$ ) and we found significant pairwise differences between species of all habitat groups (benthic-benthopelagic and benthic-pelagic both  $P<0.001$ , pelagic-benthopelagic  $P=0.015$ ). Applying the same test to each variable, we found that evolutionary rates differed significantly between habitats in five of the 12 univariate phenotypes, including caudal angle ( $Z=3.113$ ,  $P<0.001$ ), caudal ventral-lobe length ( $Z=3.406$ ,  $P<0.001$ ), dorsal base length ( $Z=2.403$ ,  $P=0.004$ ), pre-pectoral length ( $Z=3.079$ ,  $P<0.001$ ), and pre-pelvic length ( $Z=3.457$ ,  $P<0.001$ , Figure 3; Table S3). In all of these variables, evolutionary rates are lowest in pelagic species and

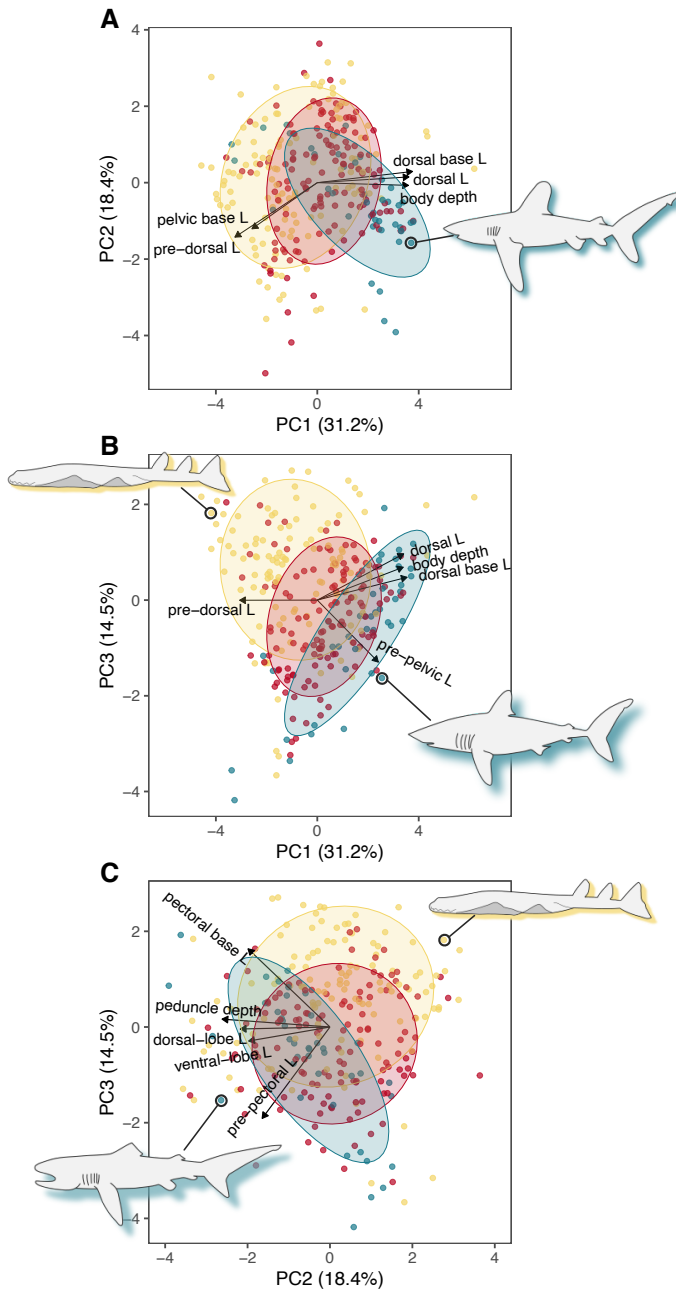


Figure 2: Shark morphospace and biplots based on a PCA of 12 morphological measurements. (A) PC2 vs. PC1, (B) PC3 vs. PC1, and (C) PC3 vs. PC2. Color corresponds to habitat (yellow: benthic; red: benthopelagic; light blue: pelagic). Arrow direction and length represent the projection through both axes and the variance attributed to each variable, respectively. Note that, for each biplot, only the 5 most important variables are projected.

highest in benthic species.

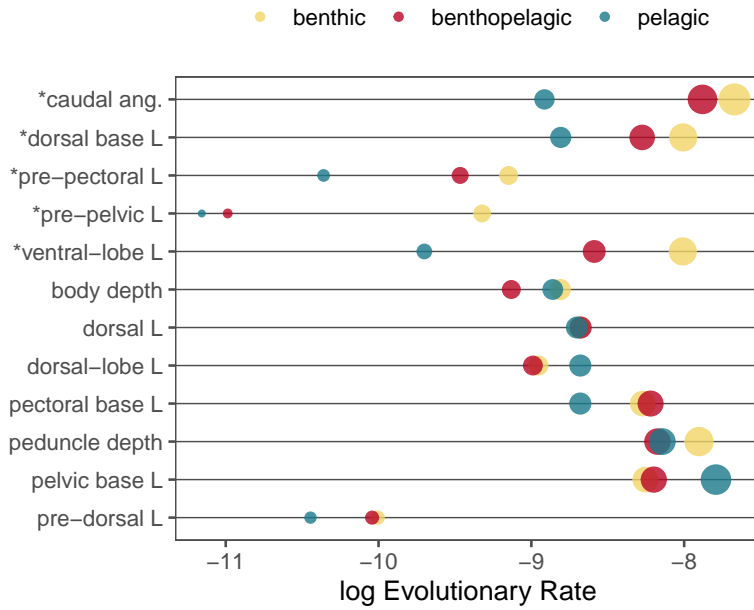


Figure 3: Log-transformed rates of phenotypic evolution across all univariate traits and habitats. Asterisks preceding trait names indicate statistical significance ( $P < 0.05$ ). Circles size reflects evolutionary rate.

### *Macroevolutionary Model Fitting*

Through our univariate phylogenetic ANOVA and evolutionary rate analysis, we found that 6 of the 12 morphological variables differed significantly between habitats in post-hoc comparisons, including body depth, caudal angle, caudal ventral lobe length, and dorsal-base, pre-pelvic, and pre-pectoral lengths. Therefore, we focused our OUwie analysis on these characters.

Our OUwie analysis of these six univariate traits revealed an OUMV model with different optima and evolutionary rates according to the three habitat regimes was the best fitting model in four traits: caudal angle, caudal ventral-lobe length, and pre-pectoral and pre-pelvic lengths. For body depth, we found an OU1 model fit best. For dorsal-base length, we found equivocal support for both an OU1 and OUM model (Figure S4).

Of those characters for which an OUM or OUMV model fit best, including equivocal models,

we found significantly discrete distributions of trait optima according to habitat regime across our distribution of  $\theta$  estimates (all THSD P<0.001; Figure 4). These include discrete optima for caudal angle, and caudal ventral lobe, dorsal-base, and pre-pectoral and pre-pelvic lengths. For caudal angle, caudal ventral lobe, and pre-pectoral and pre-pelvic lengths, our models recovered optima with the lowest values for benthic, intermediate values in benthopelagic, and highest values in pelagic lineages. For dorsal base length, optima were smallest in pelagic, intermediate in benthic, and longest in pelagic lineages.

For characters in which an OUMV model fit best, we also found strong evidence for different values of trait  $\sigma^2$  according to habitat regime (all THSD P<0.001; Figure 5). These include significant differences in  $\sigma^2$  for caudal angle, dorsal-fin base and caudal ventral lobe lengths, and pre-pectoral and pre-pelvic lengths. In all cases, pelagic lineages have the lowest  $\sigma^2$  values, benthic lineages have intermediate values, and benthopelagic lineages have the highest values.

Only four of the some 9,000 OUwie models returned negative eigenvalues and these were removed before we undertook model assessment and extracted parameter estimates. We also found that our OUwie analysis had the appropriate statistical power to distinguish more complex from simpler OUWie models. Specifically, we found that modeling each univariate trait with parameter estimates gathered during our empirical analysis resulted in similar AICc values (Figure S5) and parameter estimates (Figure S6) when compared to our empirical results.

## Discussion

We find compelling evidence that water-column habitat drives significant differences shark body shape at the macroevolutionary scale. Despite this, overall multivariate morphospace distributions of body shape are broad and therefore largely overlapping across all three habitats. These results indicate that, while habitat can drive consistent patterns of phentotypic change, all three habitats are host to a diversity of shark body shapes. Given the substantial ecological and phylogenetic diversity across our shark species, it is not surprising that we find such exten-

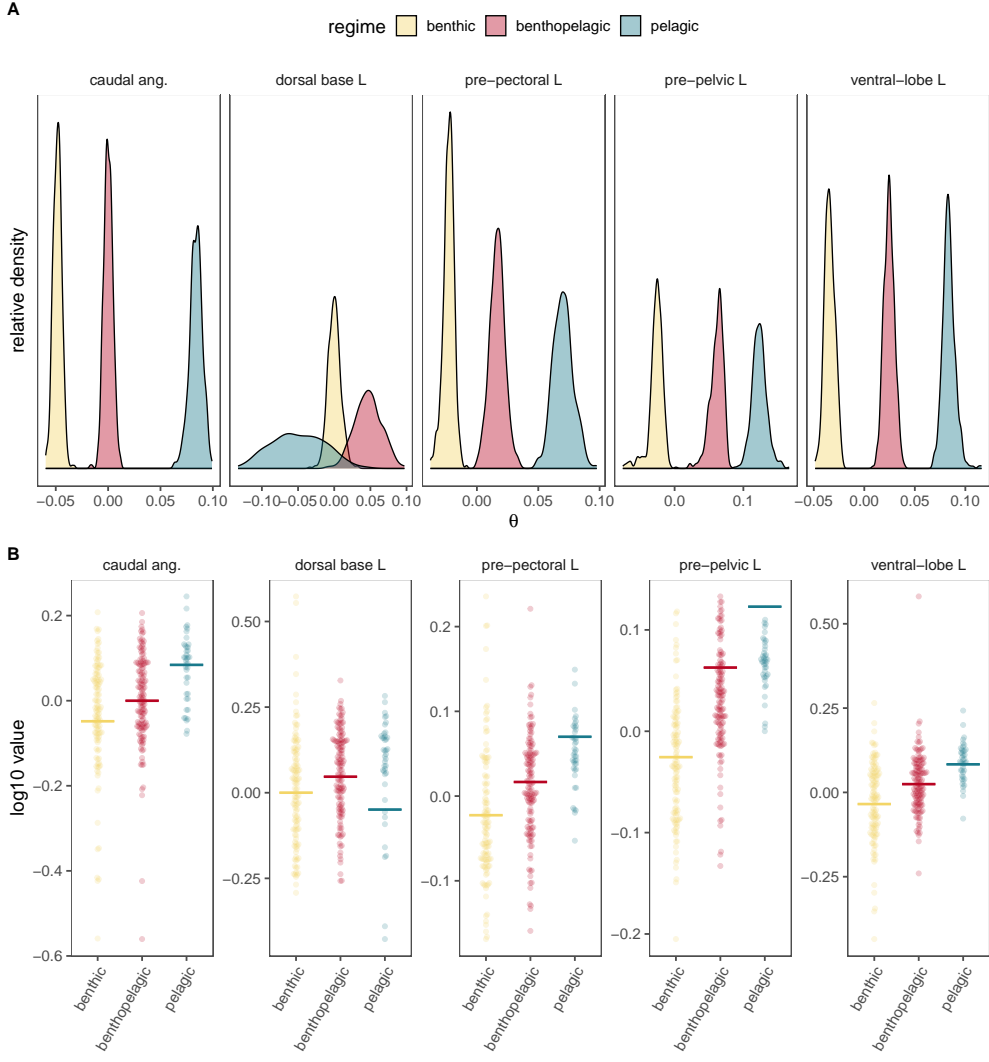


Figure 4: (A) Density distribution of optimal trait values ( $\theta$ ) across habitat regimes for body depth, heterocercal angle, dorsal-fin length, caudal dorsal-lobe length, pre-pectoral and pre-pelvic lengths, and caudal ventral-lobe length according to the best-fitting OUwie model. OUM or OUMV fit best in each case except for heterocercal angle, in which case. (B) Distribution of measured trait values and the median trait optima (solid horizontal bar) according to habitat.

sive phenotypic diversification within each habitat. Other factors aside from habitat, including trophic specialization, depth zone, reproductive mode, and phylogenetic constraints likely play additional or even more substantial roles in shark body shape diversification (Coates et al., 2018; Katona et al., 2023; López-Romero et al., 2023; Nauwelaerts et al., 2007).

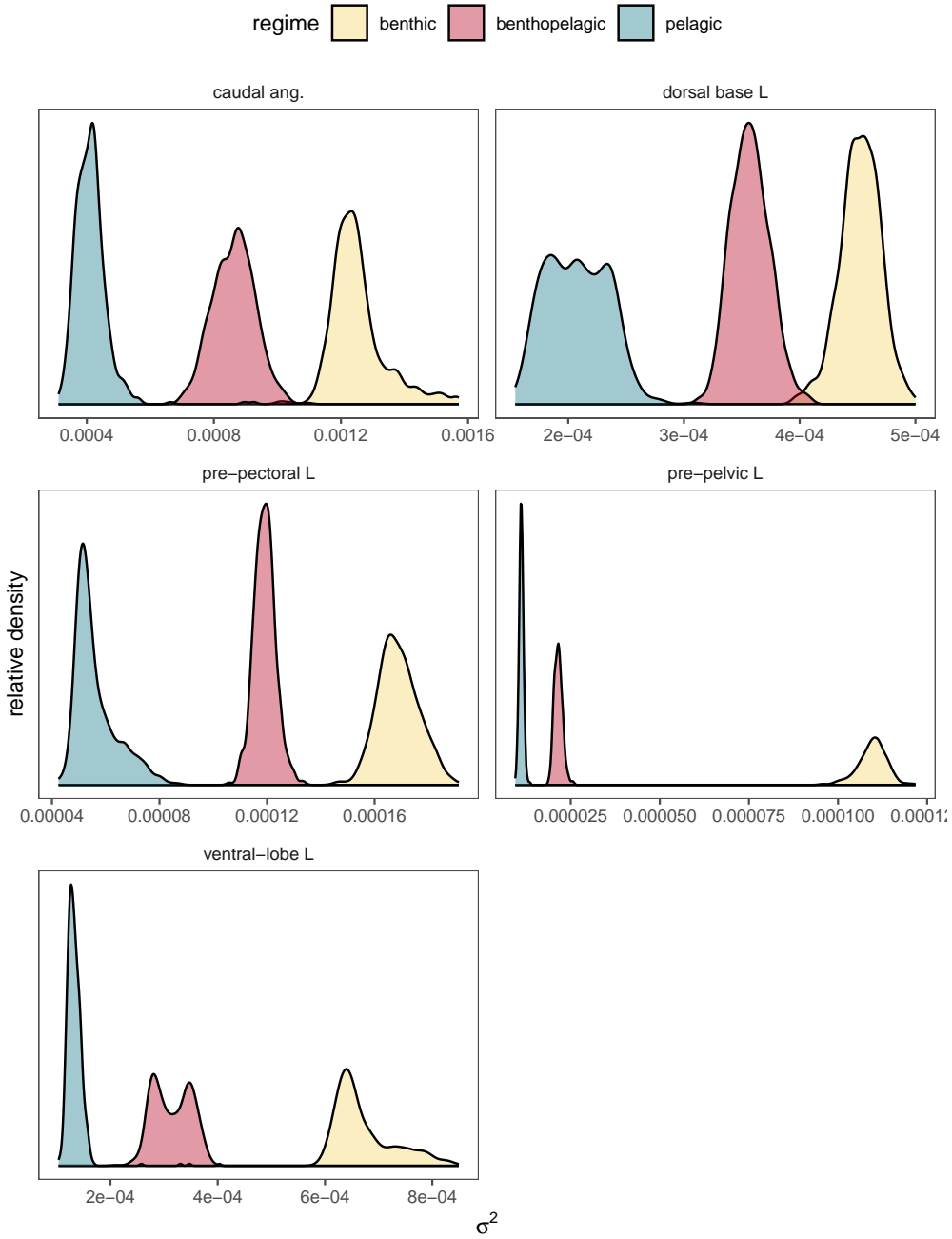


Figure 5: Density distribution of evolutionary rates ( $\sigma^2$ ) across habitat regimes for caudal-fin angle, dorsal-fin base length, pre-pectoral and pre-pelvic lengths, and ventral caudal lobe length according to the best-fitting OUwie model (OUMV in each case).

Nonetheless, we did recover consistent morphological trends in specific traits with regards to habitat regime and this alludes to the important influence water-column habitat has on the evolution of body shape in sharks. Our phylogenetic MANOVA revealed significant differences in multivariate morphology between habitats and, through our phylogenetic ANOVA tests, we found significant pairwise differences in four of the 12 univariate traits. The later includes difference between habitats in body depth, caudal ventral lobe length, and pre-pectoral and pre-pelvic lengths. The primary function of these traits is largely locomotor. Fin position and size are key determinants of swimming behavior and performance in sharks and bony fishes (Lauder, 2000). We suggest that these differences are largely consistent with the locomotor demands specific to each habitat.

Perhaps the most conspicuous patterns we uncovered are associated with (1) caudal ventral lobe length and caudal angle and (2) the position of paired fins. Specifically, for the first pattern, we uncovered a benthic-to-pelagic gradient in which the caudal ventral lobe is longer both in terms of its mean (Table S2) and trait optima and the caudal angle is increasingly larger in terms of OU optima (Figure 4). For this second pattern, we uncovered that pre-pectoral and pre-pelvic lengths are greater in terms both their mean and trait optima along the benthic-to-pelagic gradient. Although the first pattern has been reported regularly in the past (Maia et al., 2012; Thomson & Simanek, 1977), our discovery that the position of the pectoral and pelvic fins varies with habitat contrasts Thomson & Simanek (1977), who reported variation in fin position is quite small, but this finding corroborates the work of Sternes & Shimada (2020).

The kinematic motion of the caudal fin provides the sole source of locomotor thrust in selachians (Lauder & Di Santo, 2015; Maia et al., 2012; Wilga & Lauder, 2004). In the limited sharks species for which the hydrodynamics of thrust production have been studied, all of them benthopelagic or benthic species (Lauder & Di Santo, 2015), the strongly heterocercal tail accelerates water posteroventrally, resulting in a corresponding reaction force with vertically directed lift and anteriorly direct thrust components. The lift torque produced by the caudal forces only partially counteracts the anterior lift torque, resulting in a pitched body angle at all but the highest

locomotor speeds in these benthic and benthopelagic species (Lauder & Di Santo, 2015; Wilga & Lauder, 2004). In contrast, pelagic species typically swim with a much reduced body angle (Fish & Shannahan, 2000). Our gradient of caudal shape indicates that pelagic sharks, and to a lesser extent benthopelagic sharks, have more homocercal tails than benthic sharks. Coupled with greater caudal-fin angles, this results in a higher caudal fin aspect ratio, a pattern reported by other authors (Iliou et al., 2023). Furthermore, this might suggest that the more homocercal tail would produce a different wake dynamic than benthic sharks. However, the wake of homocercal caudal fins in teleosts also results in similar pattern: an anterodorsally directed reaction force, resulting in a dorsally directed lift component (Lauder, 2000; Nauen & Lauder, 2002). We therefore speculate that the combination of a larger ventral lobe and greater caudal angle in benthopelagic and especially pelagic sharks is an adaptation for the production of greater anteriorly directed reaction forces and therefore greater thrust overall, as proposed by other authors (Iliou et al., 2023; Sumikawa et al., 2024). This also represents an important adaptation for broad migration distances, cruising, and foraging strategies relying on sustained thrust and high locomotor speeds.

If benthopelagic and pelagic species have the potential to produce greater thrust and this thrust is accompanied with greater posterior lift torques, we also speculate that the position of the paired fins is a closely linked adaptation. The pectoral fins of sharks are important control surfaces and past research suggests that the function of these fins varies with habitat—pectoral fins are important in maneuvering in benthic sharks and in the generation of lift for positional and trim stability in pelagic sharks (Fish & Shannahan, 2000; Sternes et al., 2024; Wilga & Lauder, 2000). With posteriorly displaced pelvic and pectoral fins in benthopelagic and pelagic sharks in particular, it is likely that the anterior lift moments are reduced and posterior lift moments are increased. Together, the balance of lift torques may result in a reduced angle of attack and more horizontal swimming posture. We see this as an important shift in swimming hydrodynamics that reduces the frontal area of the body and in turn reduces drag (Fish & Shannahan, 2000; Thomson & Simanek, 1977). Reduced drag and a more horizontal swimming posture reduce cost

of transport (Di Santo et al., 2017) and promote more effective prey capture (Higham, 2007), respectively, both important adaptations to semi- or fully pelagic lifestyles. We note, however, that these speculative remarks do not account for differences in pelvic-fin shape and function across habitats. The shape variation and functional role of the shark pelvic fin is essentially unknown (Maia et al., 2012) and we suggested this represents an important line of future research.

We found significant differences in the rates of multivariate character evolution between all three habitats and differences in evolutionary rates of five key locomotor phenotypes: caudal angle, caudal ventral-lobe length, dorsal base length, and pre-pectoral and pre-pelvic lengths. In our multivariate rate analysis and for each of the univariate traits, rates of phenotypic evolution were lowest in benthic sharks and highest in pelagic sharks. This same pattern is corroborated by our OUwie analysis in that there is a gradient of high to low  $\sigma^2$  values across the benthic-to-pelagic axis for all five of these variables. Altogether, these patterns suggest that the benthic realm promotes and pelagic realm constrains body shape diversification especially those phenotypic traits associated with locomotion. Authors of similar macroevolutionary studies have reported the same pattern in ray-finned fishes (Burress et al., 2017; Friedman et al., 2020; Ribeiro et al., 2018) and we apply similar frameworks in explaining this trend.

The pelagic environment is largely homogenous while the benthic environment is defined by a multitude of different substrates: sand, mud, reefs, etc., each varying in its ecological and physical complexity. In addition, differences in locomotor behavior and performance are often linked to differences in feeding strategy (Higham, 2007; Rice & Hale, 2010; Webb, 1984). Feeding on pelagic prey in the open ocean requires a limited range of locomotor behavior and performance, namely cruising filter feeding or cruising and chasing (Bernal et al., 2009; Cade et al., 2020; Motta et al., 2010; Queiroz et al., 2017). Sharks inhabiting the pelagic realm therefore face few opportunities for morphological diversification and the exploration of novel niches. On the other hand, benthic sharks often employing a lie-and-wait or searching strategy (Webb, 1984) which necessarily requires physical interaction with the substrate. Furthermore, benthic sharks not only swim along the substrate in search of prey, but many often maneuver between structures

within it, altering kinematic patterns (Berio et al., 2025) and even locomotor modes, switching from swimming to a form of walking (Maia et al., 2012; Porter et al., 2022). We therefore conclude that this pattern of decreasing rates of morphological evolution along the benthic-pelagic axis reflects a pattern of decreased substrate complexity that, in turn, demands a concurrent decrease in the diversity of locomotor behavior.

Through our stochastic character mapping analysis and ancestral state reconstructions, we found compelling evidence that modern sharks have a benthic ancestor, but that this group has also transitioned to benthopelagic and pelagic realms repeatedly. We estimate that selachians have independently transitioned into the benthopelagic approximately 23 times and into the pelagic realm as many as 15 times (Figure 1). Specifically, we found that pelagic transitions occurred once in the lamniforms, seven times in the carcharhiniforms (in a common ancestor of the genus *Sphyraena*, five separate times in the genus *Carcharhinus*, and in a lineage leading to the tiger shark, *Galeocerdo cuvier*), in the whale shark, *Rhincodon typus*, four times in the squaliform family Etmopteridae, and twice within the squaliform family Dalatiidae. This contrasts the broader study of 491 species by Sternes et al. (2024) who found that transitions to the pelagic realm have occurred only 6 times.

The discrepancies in inferred habitat transitions between our study and Sternes et al. (2024) could be due to three factors: the difference in phylogenetic hypotheses used in comparative analyses, differences in habitat classifications, and the reduced number of taxa in this study. To address these first two factors simultaneously, we repeated our simmap operations and ancestral habitat reconstructions on the time-calibrated MCC tree used by Sternes et al. (2024) pruned to contain our 288 study species, but with our habitat classifications. Using the pruned MCC tree, we recovered very similar patterns of habitat transitions compared with analyses based on molecular data-only tree (Figure 1, Figure S3). Based on this, we posit that the majority of the discrepancies are due to differences in habitat classifications.

We designated many more species as benthopelagic (131 versus 61), fewer species as pelagic (41 versus 52), and many fewer species as benthic (116 versus 171). These differences in habitat

classification can be explained by a combination of two factors. First, we interpret the term "on or near bottom" to mean definitely benthopelagic. Although Sternes et al. (2024) indicate that they used the same key term in their application of benthopelagic, this framework was apparently applied inconsistently. For instance, both Compagno and Ebert indicate "on or near bottom" for the scyliorhinids *Poroderma africanum* and *P. pantherinum* and several species of the squaliform genus *Etmopterus* (e.g., *E. dislineatus*, *E. molleri*, *E. sentosus*, and *E. spinax*), yet Sternes et al. (2024) classified these species as benthic. Second, Sternes et al. (2024) classified all species of several lineages as utilizing one habitat. For example, and with important implications for the history of pelagic transitions, they classified all species of the genus *Carcharhinus* as pelagic despite definitive statements by Compagno and Ebert that would suggest a benthopelagic habitat: "bottom-dwelling" in Compagno, "sometimes at surface" in Ebert for *C. altimus*; "near bottom" in Ebert for *C. perezii*; and "shallow water close inshore on coral reefs" in Compagno, "shallow water on coral reefs and reef flats" in Ebert for *C. melanopterus*.

The discrepancies in the number of times modern sharks have transitioned to the pelagic may be cause to reinterpret some of the findings presented by Sternes et al. (2024). In particular, our findings suggest that carcharhiniforms have invaded the pelagic realm as many as seven times rather than once. Sternes et al. (2024) inferred a single carcharhiniform pelagic expansion in the branch leading to this lineage around 98.3 to 82.4 Ma in the Cenomanian to early Campanian. They also suggested that the swimming performance of sharks was enhanced due to the elevated sea temperatures that occurred 90 Ma in the Early Cretaceous (i.e, the Cretaceous Thermal Maximum, CTM; Scotese et al., 2021) and that this could have driven the pelagic expansions of both the lamniforms and carcharhiniforms.

Our analysis and reanalysis using their chosen MCC phylogenetic hypotheses suggest that carcharhiniforms probably invaded the pelagic much later. The earliest invasion was either in the lineage leading to *Galeocerdo cuvier*, no earlier than approximately 83 Ma, or in the lineage leading to the genus *Sphyrna* around 46–52 Ma. The first appearance of the genus *Galeocerdo* dates back to the early Eocene, around 56 Ma (Türtscher et al., 2021), perhaps placing the acquisition

of a pelagic lifestyle in the genus much more recent than 83 Ma. Therefore, a paleoclimatic explanation based on the CTM for the rise of pelagic sharks may apply to the laminiforms in that our analysis and that of Sternes et al. (2024) place a pelagic transition in this group no later than 124 Ma (Figure 1, Figure S3), but this explanation is unlikely for the carcharhiniforms.

The much more recent pelagic transitions in the carcharhiniforms suggest that some other factor, perhaps another paleoclimatic event, was at play. We note that the Paleocene-Eocene thermal maximum (PETM) at 56 Ma and the Early Eocene Climatic Optimum (EECO) spanning 54–49 Ma (McInerney & Wing, 2011; Scotese et al., 2021), generally coincide with the diversification of the genus *Galeocerdo* and the lineage leading to the genus *Sphyraena*, the first groups of pelagic carcharhiniforms. The PETM was a rather short but dramatic warming event, while the more prolonged EETM represents the warmest sustained interval of the Cenozoic and one of the warmest periods in Earth's history (Scotese et al., 2021). These events had drastic effects on marine ecosystems (Giusberti et al., 2016; Rivero-Cuesta et al., 2020; Speijer et al., 2012; Wilson et al., 2018); however, their effects on the macroevolutionary patterns in aquatic vertebrates is largely unexplored (Arcila & Tyler, 2017).

## Conclusion

Habitat-driven diversification in shark body shape has been the subject of many previous studies; however, ours is the first to assess the influence of habitat on the evolution of a broad range of phenotypes with locomotor significance in an explicitly phylogenetic framework. Our findings demonstrate that transitions across the benthic-pelagic habitat axis have played a central role in shaping the evolutionary tempo and trajectory of shark body shape. While overall body shape shows substantial overlap among habitat types, we find that specific traits critical to locomotion exhibit distinct habitat-associated patterns. Specifically, we found a gradient of phenotypic shifts in fin shape and placement as well as reduced rates of evolutionary change along the benthic-to-pelagic axis. These results suggest a macroevolutionary trade-off between ecologi-

cal specialization and phenotypic diversification and underscore habitat as a powerful driver of morphological evolution in aquatic vertebrates.

## Acknowledgments

We wish to thank . . .

Lastly, XX reviewers provided important critical feedback that improved the rigor of this study.

## Author contributions

XX and XX collected and analyzed data and helped write the manuscript; XX conceived the study, analyzed data, and helped write the manuscript.

## Funding

This study was funded by ....

## References

- Arcila, D. & Tyler, J.C. 2017. Mass extinction in tetraodontiform fishes linked to the palaeocene–eocene thermal maximum. *Proceedings of the Royal Society B: Biological Sciences* **284**: 20171771.
- Baken, E.K., Collyer, M.L., Kaliontzopoulou, A. & Adams, D.C. 2021. geomorph v4. 0 and gmshiny: Enhanced analytics and a new graphical interface for a comprehensive morphometric experience. *Methods in Ecology and Evolution* **12**: 2355–2363.
- Beaulieu, J.M. & O'Meara, B. 2024. *OUwie: Analysis of Evolutionary Rates in an OU Framework*. URL <https://github.com/thej022214/OUwie>. R package version 2.13.

Berio, F., Morerod, C. & Di Santo, V. 2025. Speed-dependent locomotor patterns during steady swimming in a demersal shark. *Journal of Fish Biology* .

Bernal, D., Sepulveda, C., Musyl, M. & Brill, R. 2009. The eco-physiology of swimming and movement patterns of tunas, billfishes, and large pelagic sharks. In: *Fish Locomotion: An Etho-ecological Approach* (P. Domenici & B. Kapoor, eds), pp. 437–483. Enfield Scientific Publishers, Enfield, NH.

Boettiger, C., Coop, G. & Ralph, P. 2012. Is your phylogeny informative? Measuring the power of comparative methods. *Evolution* **66**: 2240–2251.

Burress, E.D., Holcomb, J.M., Tan, M. & Armbruster, J.W. 2017. Ecological diversification associated with the benthic-to-pelagic transition by North American minnows. *Journal of Evolutionary Biology* **30**: 549–560.

Cade, D.E., Levenson, J.J., Cooper, R., de la Parra, R., Webb, D.H. & Dove, A.D. 2020. Whale sharks increase swimming effort while filter feeding, but appear to maintain high foraging efficiencies. *Journal of Experimental Biology* **223**: jeb224402.

Coates, M.I., Finarelli, J.A., Sansom, I.J., Andreev, P.S., Criswell, K.E., Tietjen, K., Rivers, M.L. & La Riviere, P.J. 2018. An early chondrichthyan and the evolutionary assembly of a shark body plan. *Proceedings of the Royal Society B: Biological Sciences* **285**: 20172418.

Compagno, L.J. 1984. *FAO Species Catalogue. Vol. 4. Sharks of the World. an Annotated and Illustrated Catalogue of Shark Species Known to Date*. FAO.

Cooper, N., Thomas, G.H., Venditti, C., Meade, A. & Freckleton, R.P. 2016. A cautionary note on the use of Ornstein Uhlenbeck models in macroevolutionary studies. *Biological Journal of the Linnean Society* **118**: 64–77.

Di Santo, V., Kenaley, C.P. & Lauder, G.V. 2017. High postural costs and anaerobic metabolism

- during swimming support the hypothesis of a u-shaped metabolism–speed curve in fishes. *Proceedings of the National Academy of Sciences* **114**: 13048–13053.
- Ebert, D.A., Dando, M. & Fowler, S. 2021. *Sharks of the World: A Complete Guide*, vol. 19. Princeton University Press.
- Fish, F. & Shannahan, L. 2000. The role of the pectoral fins in body trim of sharks. *Journal of Fish Biology* **56**: 1062–1073.
- Friedman, S., Price, S., Corn, K., Larouche, O., Martinez, C. & Wainwright, P. 2020. Body shape diversification along the benthic–pelagic axis in marine fishes. *Proceedings of the Royal Society B* **287**: 20201053.
- Garland Jr, T., Dickerman, A.W., Janis, C.M. & Jones, J.A. 1993. Phylogenetic analysis of covariance by computer simulation. *Systematic Biology* **42**: 265–292.
- Gayford, J.H., Whitehead, D.A., Ketchum, J.T. & Field, D.J. 2023. The selective drivers of allometry in sharks (Chondrichthyes: Elasmobranchii). *Zoological Journal of the Linnean Society* **198**: 257–277.
- Giusberti, L., Boscolo Galazzo, F. & Thomas, E. 2016. Variability in climate and productivity during the Paleocene–Eocene Thermal Maximum in the western Tethys (Forada section). *Climate of the Past* **12**: 213–240.
- Gleiss, A.C., Potvin, J. & Goldbogen, J.A. 2017. Physical trade-offs shape the evolution of buoyancy control in sharks. *Proceedings of the Royal Society B: Biological Sciences* **284**: 20171345.
- Higham, T.E. 2007. The integration of locomotion and prey capture in vertebrates: morphology, behavior, and performance. *Integrative and Comparative Biology* **47**: 82–95.
- Ho, L.S.T. & Ané, C. 2014. Intrinsic inference difficulties for trait evolution with Ornstein–Uhlenbeck models. *Methods in Ecology and Evolution* **5**: 1133–1146.

- Hulsey, C., Roberts, R., Loh, Y.H., Rupp, M. & Streelman, J. 2013. Lake Malawi cichlid evolution along a benthic/limnetic axis. *Ecology and Evolution* **3**: 2262–2272.
- Iliou, A.S., Vanderwright, W., Harding, L., Jacoby, D.M., Payne, N.L. & Dulvy, N.K. 2023. Tail shape and the swimming speed of sharks. *Royal Society Open Science* **10**: 231127.
- Katona, G., Szabó, F., Végvári, Z., Székely Jr, T., Liker, A., Freckleton, R.P., Vági, B. & Székely, T. 2023. Evolution of reproductive modes in sharks and rays. *Journal of Evolutionary Biology* **36**: 1630–1640.
- Lauder, G.V. 2000. Function of the caudal fin during locomotion in fishes: kinematics, flow visualization, and evolutionary patterns. *American Zoologist* **40**: 101–122.
- Lauder, G.V. & Di Santo, V. 2015. Swimming mechanics and energetics of elasmobranch fishes. In: *Fish physiology*, vol. 34, pp. 219–253. Elsevier.
- López-Romero, F.A., Stumpf, S., Kämplinga, P., Böhmer, C., Pradel, A., Brazeau, M.D. & Kriwet, J. 2023. Shark mandible evolution reveals patterns of trophic and habitat-mediated diversification. *Communications Biology* **6**: 496.
- Maia, A.M., Wilga, C.A. & Lauder, G.V. 2012. Biomechanics of locomotion in sharks, rays, and chimaeras. *Biology of Sharks and Their Relatives* **1**: 125–51.
- Martinez, C.M., Friedman, S.T., Corn, K.A., Larouche, O., Price, S.A. & Wainwright, P.C. 2021. The deep sea is a hot spot of fish body shape evolution. *Ecology Letters* **24**: 1788–1799.
- McInerney, F.A. & Wing, S.L. 2011. The Paleocene-Eocene Thermal Maximum: A perturbation of carbon cycle, climate, and biosphere with implications for the future. *Annual Review of Earth and Planetary Sciences* **39**: 489–516.
- Miller, E.C., Faucher, R., Hart, P.B., Rincón-Sandoval, M., Santaquiteria, A., White, W.T., Baldwin, C.C., Miya, M., Betancur-R, R., Tornabene, L. et al. 2025. Reduced evolutionary constraint

accompanies ongoing radiation in deep-sea anglerfishes. *Nature Ecology & Evolution* **9**: 474–490.

Motta, P.J., Maslanka, M., Hueter, R.E., Davis, R.L., De la Parra, R., Mulvany, S.L., Habegger, M.L., Strother, J.A., Mara, K.R., Gardiner, J.M. et al. 2010. Feeding anatomy, filter-feeding rate, and diet of whale sharks *Rhincodon typus* during surface ram filter feeding off the Yucatan Peninsula, Mexico. *Zoology* **113**: 199–212.

Nauen, J.C. & Lauder, G.V. 2002. Hydrodynamics of caudal fin locomotion by chub mackerel, *Scomber japonicus* (Scombridae). *Journal of Experimental Biology* **205**: 1709–1724.

Nauwelaerts, S., Wilga, C., Sanford, C. & Lauder, G. 2007. Hydrodynamics of prey capture in sharks: effects of substrate. *Journal of the Royal Society Interface* **4**: 341–345.

Pennell, M.W., Eastman, J.M., Slater, G.J., Brown, J.W., Uyeda, J.C., Fitzjohn, R.G., Alfaro, M.E. & Harmon, L.J. 2014. geiger v2.0: an expanded suite of methods for fitting macroevolutionary models to phylogenetic trees. *Bioinformatics* **30**: 2216–2218. doi:10.1093/bioinformatics/btu181.

Pike, N. 2011. Using false discovery rates for multiple comparisons in ecology and evolution. *Methods in ecology and Evolution* **2**: 278–282.

Pinheiro, J.C. & Bates, D.M. 2000. *Mixed-Effects Models in S and S-PLUS*. Springer, New York. doi:10.1007/b98882.

Porter, M.E., Hernandez, A.V., Gervais, C.R. & Rummer, J.L. 2022. Aquatic walking and swimming kinematics of neonate and juvenile epaulette sharks. *Integrative and comparative biology* **62**: 1710–1724.

Queiroz, N., Vila-Pouca, C., Couto, A., Southall, E.J., Mucientes, G., Humphries, N.E. & Sims, D.W. 2017. Convergent foraging tactics of marine predators with different feeding strategies across heterogeneous ocean environments. *Frontiers in Marine Science* **4**: 239.

R Core Team 2022. *R: A Language and Environment for Statistical Computing*. R Foundation for Statistical Computing, Vienna, Austria. URL <https://www.R-project.org/>.

Revell, L.J. 2024. phytools 2.0: an updated R ecosystem for phylogenetic comparative methods (and other things). *PeerJ* **12**: e16505. doi:10.7717/peerj.16505.

Ribeiro, E., Davis, A.M., Rivero-Vega, R.A., Ortí, G. & Betancur-R, R. 2018. Post-cretaceous bursts of evolution along the benthic-pelagic axis in marine fishes. *Proceedings of the Royal Society B* **285**: 20182010.

Rice, A.N. & Hale, M.E. 2010. Roles of locomotion in feeding. In: *Fish Locomotion: An Ethological Perspective* (P. Domenici & B. Kapoor, eds), pp. 171–199. CRC Press.

Rivero-Cuesta, L., Westerhold, T. & Alegret, L. 2020. The late lutetian thermal maximum (middle eocene): first record of deep-sea benthic foraminiferal response. *Palaeogeography, Palaeoclimatology, Palaeoecology* **545**: 109637.

Schindelin, J., Arganda-Carreras, I., Frise, E. & Kaynig, e.a. 2012. Fiji: an open-source platform for biological-image analysis. *Nature Methods* **9**: 676–682.

Scotese, C.R., Song, H., Mills, B.J. & van der Meer, D.G. 2021. Phanerozoic paleotemperatures: The earth's changing climate during the last 540 million years. *Earth-Science Reviews* **215**: 103503.

Speijer, R., Scheibner, C., Stassen, P. & Morsi, A.M.M. 2012. Response of marine ecosystems to deep-time global warming: a synthesis of biotic patterns across the paleocene-eocene thermal maximum (petm). *Austrian Journal of Earth Sciences* **105**: 6–16.

Stein, R.W., Mull, C.G., Kuhn, T.S., Aschliman, N.C., Davidson, L.N., Joy, J.B., Smith, G.J., Dulvy, N.K. & Mooers, A.O. 2018. Global priorities for conserving the evolutionary history of sharks, rays and chimaeras. *Nature Ecology & Evolution* **2**: 288–298.

- Sternes, P.C., Schmitz, L. & Higham, T.E. 2024. The rise of pelagic sharks and adaptive evolution of pectoral fin morphology during the Cretaceous. *Current Biology* **34**: 2764–2772.
- Sternes, P.C. & Shimada, K. 2020. Body forms in sharks (Chondrichthyes: Elasmobranchii) and their functional, ecological, and evolutionary implications. *Zoology* **140**: 125799.
- Sumikawa, H., Naraoka, Y., Obayashi, Y., Fukue, T. & Miyoshi, T. 2024. Fluid dynamic properties of shark caudal fin morphology and its relationship to habitats. *Ichthyological Research* **71**: 294–304.
- Thomson, K.S. & Simanek, D.E. 1977. Body form and locomotion in sharks. *American Zoologist* **17**: 343–354.
- Türtscher, J., López-Romero, F.A., Jambura, P.L., Kindlimann, R., Ward, D.J. & Kriwet, J. 2021. Evolution, diversity, and disparity of the tiger shark lineage *galeocerdo* in deep time. *Paleobiology* **47**: 574–590.
- Webb, P.W. 1984. Body form, locomotion and foraging in aquatic vertebrates. *American zoologist* **24**: 107–120.
- Wilga, C. & Lauder, G. 2004. Hydrodynamic function of the shark's tail. *Nature* **430**: 850–850.
- Wilga, C. & Lauder, G.V. 2000. Three-dimensional kinematics and wake structure of the pectoral fins during locomotion in leopard sharks *triakis semifasciata*. *Journal of Experimental Biology* **203**: 2261–2278.
- Wilson, J., Monteiro, F., Schmidt, D., Ward, B. & Ridgwell, A. 2018. Linking marine plankton ecosystems and climate: a new modeling approach to the warm early Eocene climate. *Paleceanography and Paleoclimatology* **33**: 1439–1452.

## **Supplementary Information**

### *Data availability*

Scripts and data are available at [http://datadryad.org/share/sKBbmgG5G6K\\_7vPrCPMU0ickRC](http://datadryad.org/share/sKBbmgG5G6K_7vPrCPMU0ickRC)  
AomCgj44WLUuuHYhI.

Table S1: Results and model-fit metrics of phylogenetic generalized least squares regression for each of the 12 variables bases on Brownian motion (BM) and Ornstein-Uhlenbeck (OU) correlation structures. For each variable, models are ranked according to corrected AIC (AICc) and AICc weight

Variable	model	Slope	df	P value	AICc	weight
body depth	BM	1.02	3	<0.001	-638.16	1.00
	OU	1.20	4		-504.44	0.00
peduncle depth	BM	1.02	3	<0.001	-379.12	1.00
	OU	1.06	4		-334.13	0.00
dorsal-lobe length	BM	1.06	3	<0.001	-630.62	1.00
	OU	1.09	4		-362.61	0.00
ventral-lobe length	BM	1.14	3	<0.001	-476.11	1.00
	OU	1.16	4		-463.79	0.00
dorsal base length	BM	1.00	3	<0.001	-425.00	1.00
	OU	1.18	4		-318.99	0.00
pectoral base length	BM	1.03	3	<0.001	-449.08	1.00
	OU	1.12	4		-401.48	0.00
pelvic base length	BM	1.06	3	<0.001	-407.26	1.00
	OU	0.96	4		-345.69	0.00
pre-dorsal length	BM	1.01	3	<0.001	-961.64	1.00
	OU	0.97	4		-461.03	0.00
pre-pelvic length	BM	0.98	3	<0.001	-937.86	1.00
	OU	1.05	4		-788.25	0.00
pre-pectoral length	BM	0.98	3	<0.001	-767.75	1.00
	OU	1.02	4		-712.66	0.00
dorsal length	BM	1.09	3	<0.001	-561.21	1.00
	OU	1.23	4		-378.12	0.00
caudal ang.	OU	0.15	4	<0.001	-394.02	1.00

BM	-0.05	3	-356.57	0.00
----	-------	---	---------	------

Table S2: Simulation-based phylogenetic ANOVA results. Procedures for each variable were based on 10,000 simulations. For each variable, post-hoc comparison P values appear in the right of the table. Significant overall and pairwise P values are bolded

Variable	F	P value	Pairwise P values		
			habitat	benthopelagic	pelagic
body depth	17.473	0.075	benthic	0.637	<b>0.024</b>
			benthopelagic		<b>0.024</b>
caudal ang.	12.964	0.148	benthic	0.459	0.129
			benthopelagic		0.146
dorsal length	3.5698	0.601	benthic	0.836	0.562
			benthopelagic		0.562
dorsal base length	4.287	0.553	benthic	0.629	0.629
			benthopelagic		0.818
dorsal-lobe length	9.578	0.241	benthic	0.513	0.232
			benthopelagic		0.232
pectoral base length	6.441	0.393	benthic	0.674	0.674
			benthopelagic		0.797
peduncle depth	3.541	0.611	benthic	0.587	0.587
			benthopelagic		0.587
pelvic base length	12.991	0.146	benthic	0.319	0.146
			benthopelagic		0.298
pre-dorsal length	15.098	0.109	benthic	0.209	0.209
			benthopelagic		0.980
pre-pectoral length	21.283	0.043	benthic	0.186	<b>0.037</b>
			benthopelagic		0.156
pre-pelvic length	64.717	<0.001	benthic	<b>0.002</b>	<0.001
			benthopelagic		0.076

ventral-lobe length	22.663	<b>0.036</b>	benthic	0.145	<b>0.033</b>
			benthopelagic	0.145	

---

Table S3: Results of simulation-based comparisons of evolutionary rates among habitat groups. Procedures for each variable were based on 10,000 simulations. For each variable, relative rate ratios and pairwise P values are appear to the right of the table. Significant overall and pairwise P values are bolded

Variable	Z	P value	Pairwise P-value		
			benthic	benthopelagic	pelagic
body depth	0.446	0.341	benthic	0.076	0.842
			benthopelagic		0.281
caudal ang.	3.113	<0.001	benthic	0.238	<b>&lt;0.001</b>
			benthopelagic		<b>&lt;0.001</b>
dorsal-lobe length	0.382	0.364	benthic	0.838	0.289
			benthopelagic		0.221
ventral-lobe length	3.406	<0.001	benthic	<b>0.001</b>	<b>&lt;0.001</b>
			benthopelagic		<b>&lt;0.001</b>
dorsal-fin length	-2.109	0.993	benthic	0.956	0.953
			benthopelagic		0.919
dorsal base length	2.403	0.004	benthic	0.140	<b>0.002</b>
			benthopelagic		<b>0.038</b>
pectoral base length	1.220	0.121	benthic	0.771	0.118
			benthopelagic		0.073
pelvic base length	1.225	0.120	benthic	0.759	0.077
			benthopelagic		0.111
peduncle depth	0.124	0.452	benthic	0.135	0.354
			benthopelagic		0.901
pre-dorsal length	1.118	0.143	benthic	0.836	0.091
			benthopelagic		0.114
pre-pectoral length	3.079	<0.001	benthic	0.079	<b>&lt;0.001</b>
			benthopelagic		<b>&lt;0.001</b>

pre-pelvic length	3.457	<0.001	benthic	<0.001	<0.001
			benthopelagic		0.504

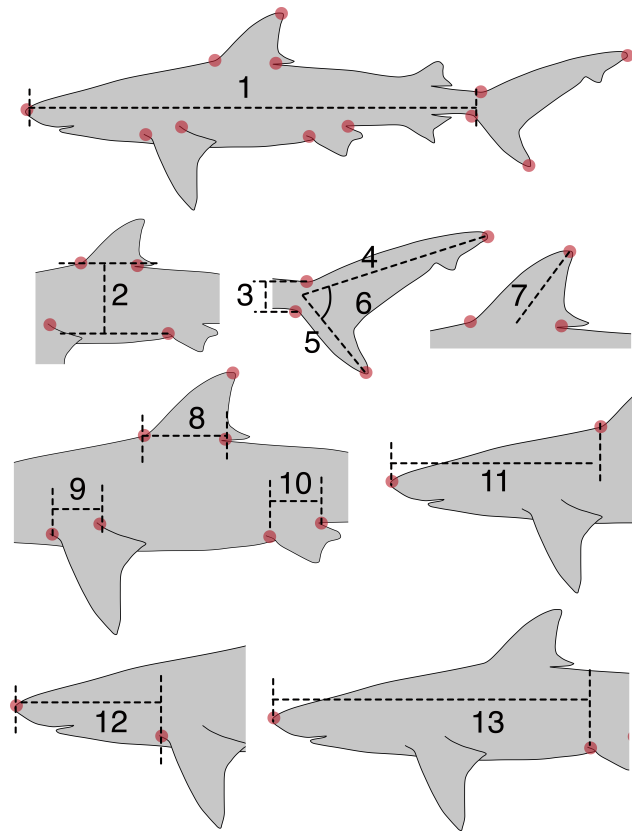


Figure S1: Morphometric measurements based on 12 homologous points used in this study (and their abbreviations throughout). 1, pre-caudal length (PCL); 2, body depth; 3, peduncle depth; 4, caudal dorsal lobe length (dorsal-lobe L); 5, ventral dorsal lobe length (ventral-lobe L); 6, caudal angle; 7, dorsal-fin length (dorsal L); 8, dorsal-fin base length (dorsal base L); 9, pectoral-fin base length (pectoral base L); 10, pelvic-fin base length (pelvic base L); 11, pre-dorsal length (pre-dorsal L); 12, pre-pectoral length (pre-pectoral L); and 13, pre-pelvic length (pre-pelvic L).

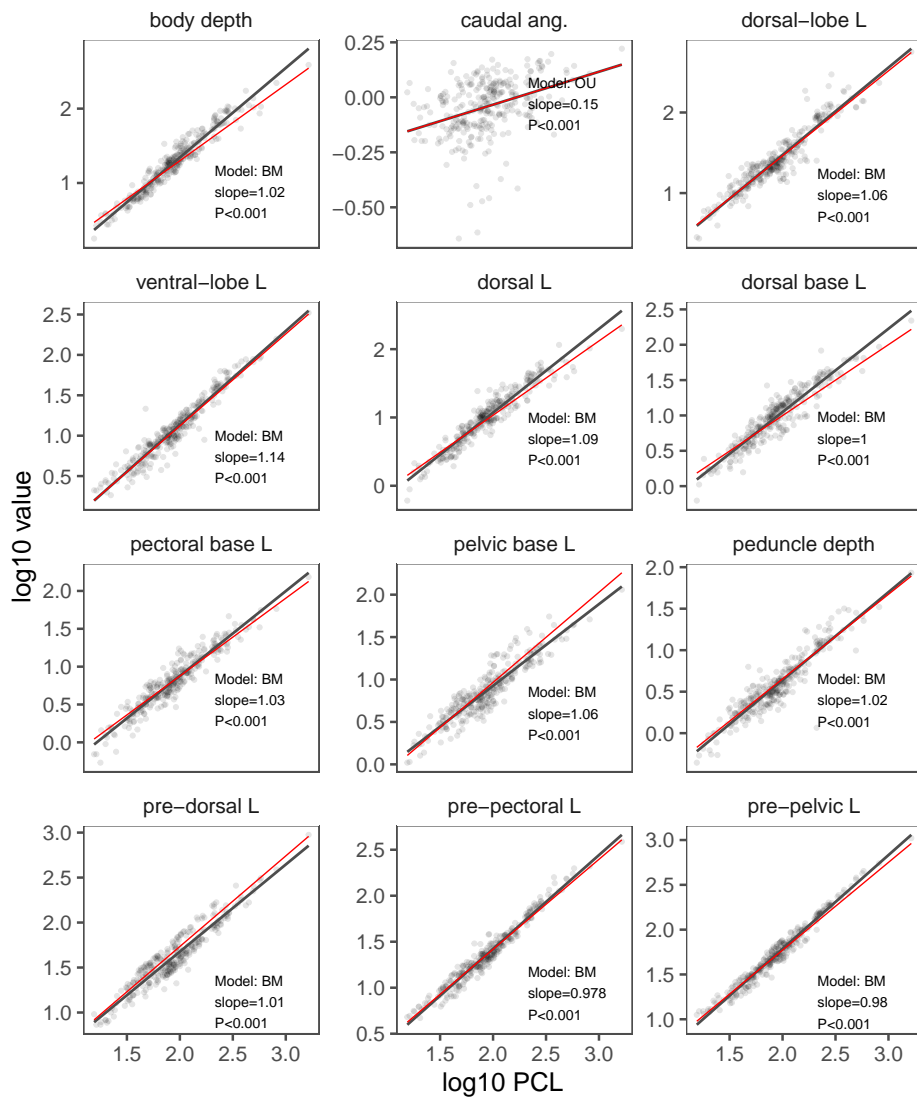


Figure S2: Scatter plots of all 12 transformed log<sub>10</sub> body-shape variables vs. log<sub>10</sub> pre-length (PCL). Black regression lines represent linear predictions without phylogenetic correction, while red lines represent predictions from phylogenetic generalized least squares (PGLS) modeling. Inset text report the best-fitting correlation model (either Brownian motion (BM) or Ornstein-Uhlenbeck (OU)), PGLS slope, and P value. See Table S1 for model fit metrics.

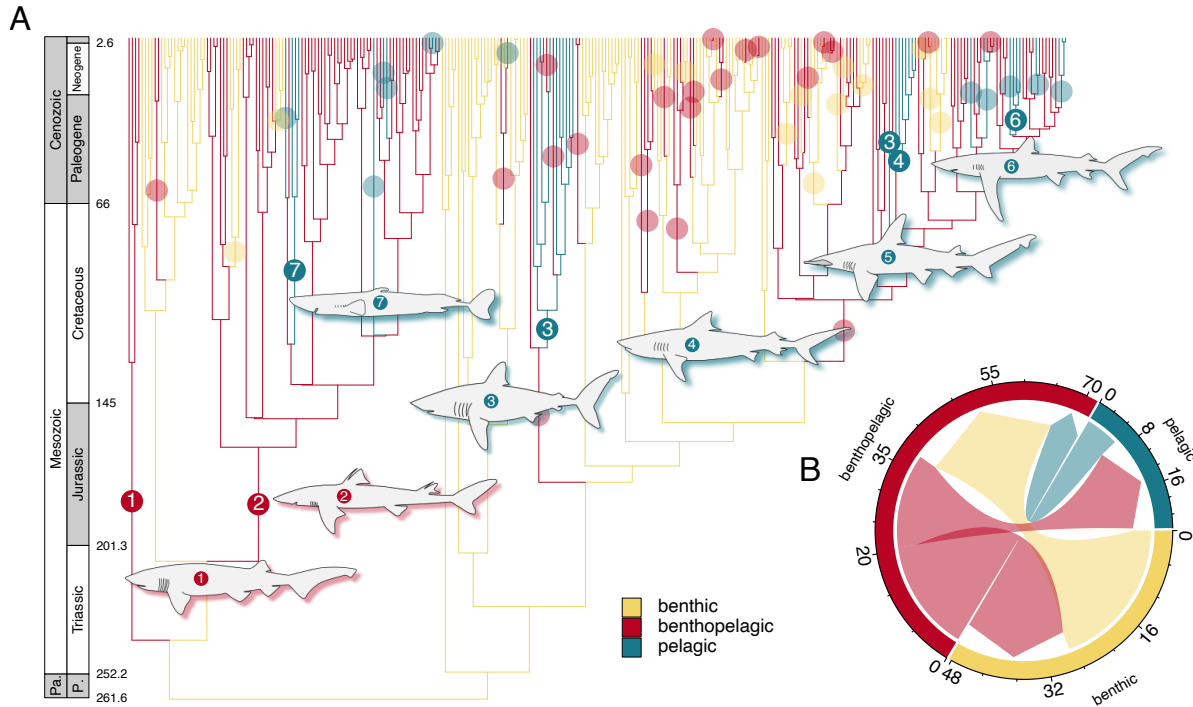


Figure S3: (A) Majority-rule consensus, fossil-calibrated time tree from (Stein et al., 2018) pruned to contain our 288 study species. Edge colors represent habitat states and transparent circles represent state transitions across the phylogeny based on ancestral state reconstructions from 500 simmap procedures. Opaque, numbered circles represent major habitat transitions: 1, a benthopelagic transition in the branch leading to the Hexanchiformes; 2, a benthopelagic transition in the branch leading to the Squaliformes; 3, pelagic transition in the branch leading to the Laminiformes minus *Mitsukurina*; 4, pelagic transition in the branch leading to the genus *Sphyrna*; 5, a pelagic transition in the branch leading *Galeocerdo cuvier*; 6, a pelagic transition in the branch leading to a clade of *Prionace glauca* and several species of the genus *Carcharhinus*; and 7, a pelagic transition in the branch leading to a clade of deep-sea squaliforms of the genera *Euprotomicrus* and *Squaliolus*. Body-outline drawings represent species included in lineages that have undergone each of the major habitat shifts. (B) Chord diagram representing the the mean number of transitions into and out of each habitat state from the 500 simmap trees.

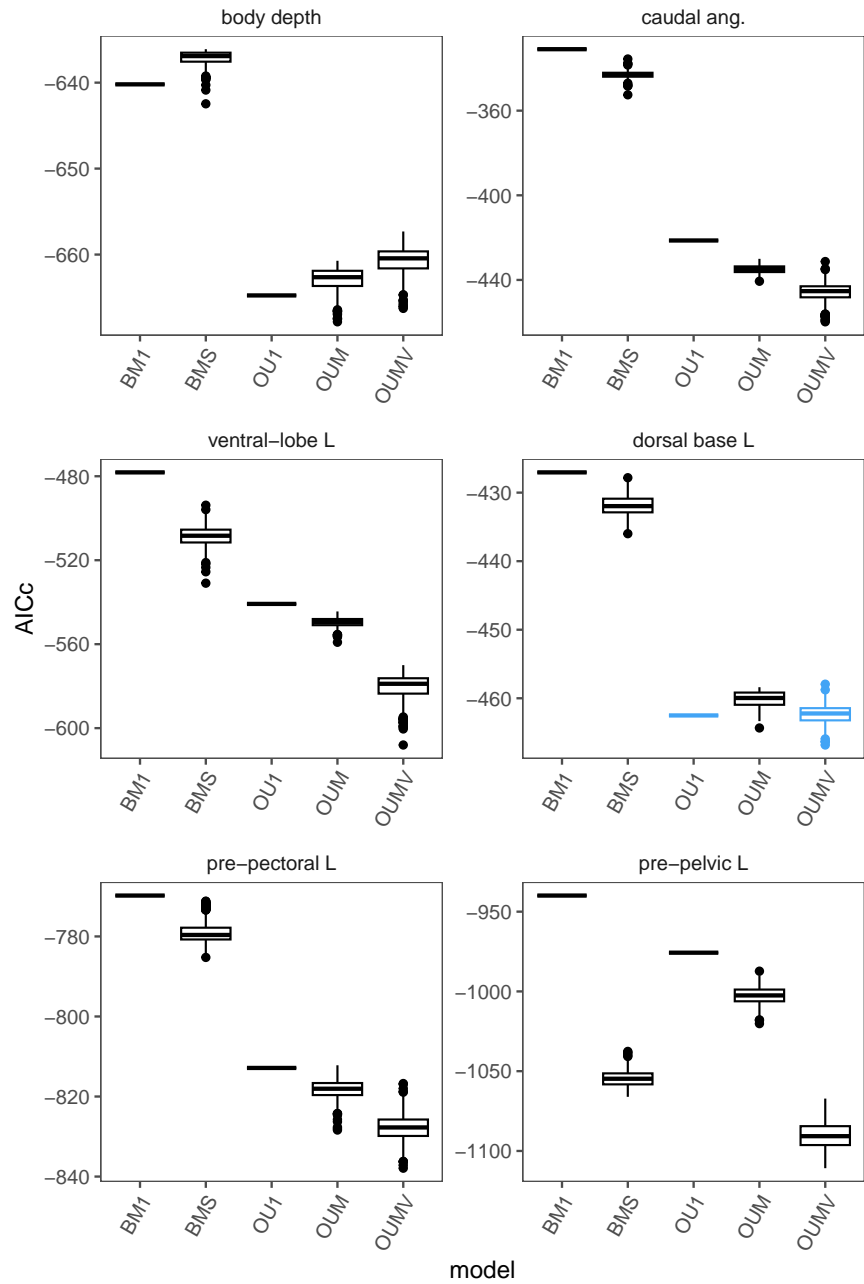


Figure S4: Boxplots representing median (horizontal bars), interquartile range (boxes) and 1.5 time the interquartile range (whiskers) of AICc scores from macroevolutionary models fitting in OUwie. The color blue indicates roughly equivalent models -the best fitting models and others whose median AICc scores were within 2 units of that model. Note that BM1 and OU1 models were evaluated only once for each variable and thus have only one AICc value.

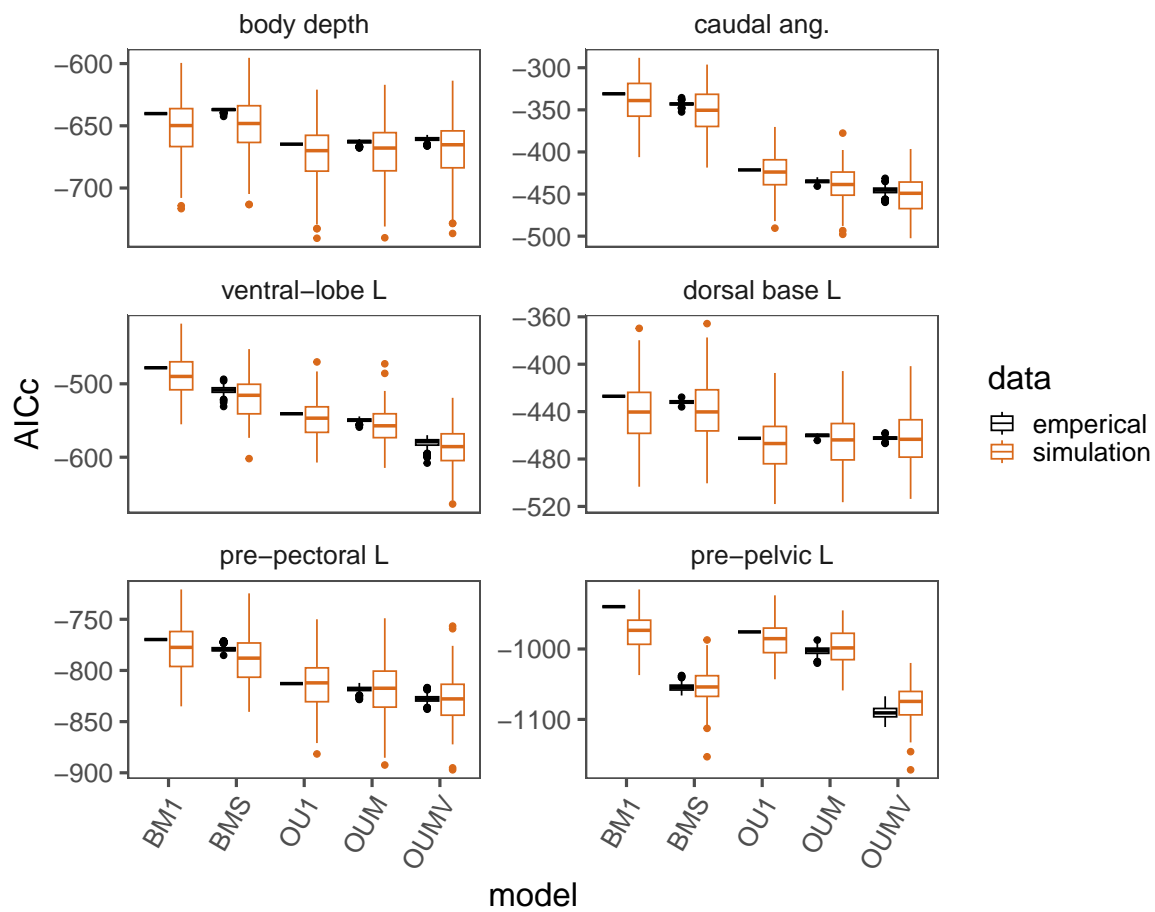


Figure S5: Boxplots comparing AICc values of OUwie models constructed during our empirical analysis and those constructed with simulated data across univariate traits.

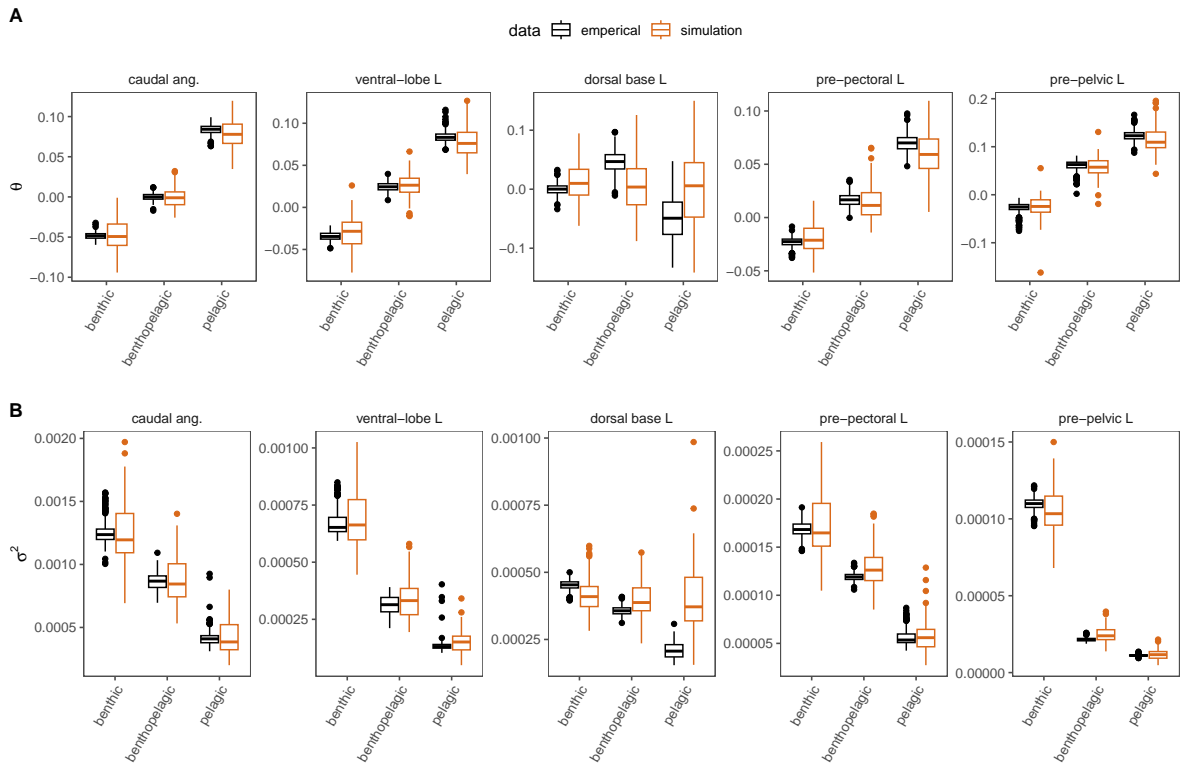


Figure S6: Boxplots comparing  $\theta$  (A) and  $\sigma^2$  (B) values returned by OUwie models constructed during our empirical analysis and those constructed with simulated data.